Development of a brushless HTS exciter for a 10 kW HTS synchronous generator

OPEN ACCESS
IOP Publishing
Superconductor Science and Technology
Supercond. Sci. Technol. **29** (2016) 024008 (11pp)
doi:10.1088/0953-2048/29/2/024008

Development of a brushless HTS exciter for a 10 kW HTS synchronous generator

Chris W Bumby[1], Rodney A Badcock[1], Hae-Jin Sung[2], Kwang-Min Kim[2], Zhenan Jiang[1], Andres E Pantoja[1], Patrick Bernardo[1,3], Minwon Park[2] and Robert G Buckley[1]

[1] Robinson Research Institute, Victoria University of Wellington, 69 Gracefield Road, PO Box 33-436, Lower Hutt 5046, New Zealand
[2] Changwon National University, 20 Changwondaehak-ro, Uichang-gu, Changwon-si, Gyeongsangnam-do, Korea
[3] South Westphalia University of Applied Sciences, Lindenstraße 53, D-59872 Meschede, Germany

E-mail: chris.bumby@vuw.ac.nz

Received 31 August 2015, revised 12 November 2015
Accepted for publication 30 November 2015
Published 12 January 2016

Abstract

HTS synchronous generators, in which the rotor coils are wound from high-T_c superconducting wire, are exciting attention due to their potential to deliver very high torque and power densities. However, injection of the large DC currents required by the HTS rotor coils presents a technical challenge. In this paper we discuss the development of a brushless HTS exciter which operates across the cryostat wall to inject a superconducting DC current into the rotor coil circuit. This approach fundamentally alters the thermal load upon the cryogenic system by removing the need for thermally inefficient normal-conducting current leads. We report results from an experimental laboratory device and show that it operates as a constant voltage source with an effective internal resistance. We then discuss the design of a prototype HTS-PM exciter based on our experimental device, and describe its integration with a demonstration HTS generator. This 200 RPM, 10 kW synchronous generator comprises eight double pancake HTS rotor coils which are operated at 30 K, and are energised to 1.5 T field through the injection of 85 A per pole. We show how this excitation can be achieved using an HTS-PM exciter consisting of 12 stator poles of 12 mm YBCO coated-conductor wire and an external permanent magnet rotor. We demonstrate that such an exciter can excite the rotor windings of this generator without forming a thermal-bridge across the cryostat wall. Finally, we provide estimates of the thermal load imposed by our prototype HTS-PM exciter on the rotor cryostat. We show that duty cycle operation of the device ensures that this heat load can be minimised, and that it is substantially lower than that of equivalently-rated conventional current leads.

Keywords: HTS generator, HTS flux pump, brushless exciter, dynamic resistance, HTS dynamo, rotating cryostat

(Some figures may appear in colour only in the online journal)

1. Introduction

In recent years there has been an increasing drive to develop large-capacity, high-energy density generators for a variety of applications including: off-shore wind-turbines [1], direct-drive high speed generators [2], ship motors [3, 4] and on-board generators [5]. All these applications require high-torque density machines which are achieved through developing large magnetic fields within the rotor coils of a synchronous machine. The high current density and low loss of high temperature superconducting (HTS) wire makes it attractive for these applications, as HTS rotor coil windings result in greater power density (lower weight and size) and improved

electrical stability compared to conventional machines [6–8]. International manufacturers who are actively developing superconducting machines include: Doosan HE [9] (wind and ship); Guina R&D [10]; Kawasaki HI [11, 12] (ship); Oswald [13] (motor); POSCO [14] (wind); Teco-Westinghouse [15] (wind) and Siemens [16] (utilities generator).

The rotor of a synchronous HTS machine consists of two or more HTS race-track coils which can generate stator-rotor gap fields in excess of 1 T. In order to generate these fields, large currents [17, 18] (often $>$100 A) must be injected into the rotor coils. This requires that the rotor cryostat must be penetrated by at least two metal current leads which carry current from ambient temperature to the cryogenic environment. These DC current leads impose a substantial thermal load upon the cryogenic system, due to both ohmic heating and thermal conduction effects [19]. The incurred cooling requirements lead to significant additional capital and operating costs [7] for these machines.

An additional problem for the design of synchronous HTS machines is the transfer of large DC currents across a rotating joint, in order to excite the HTS rotor coils. Existing excitation technologies such as slip-rings [20] and high-frequency brushless-exciters [21, 22] all reduce performance and increase cost and complexity. Slip-ring contacts can suffer from arc erosion at high currents [23], and they are unsuited for operation at high speeds ($\gtrapprox$1000 rpm), as they wear rapidly at high rpm [24]. Inductive brushless-exciters [25] require high-stability switched-mode power electronics to be mounted upon the rotor if large DC currents are to be injected. This is generally unsuitable for high-speed operation, and can reduce the machine's overall power density, reliability and ease of maintenance.

An alternative approach to inject current into a set of HTS rotor coils is through the use of a superconducting flux pump. Flux pumps [26–31] are a class of device which enable a DC current to be pumped around a closed superconducting circuit without the need for direct electrical connection to a power supply. This eliminates the thermal penalties associated with metal current leads. In this paper we present a novel design for a rotating flux pump exciter which is capable of injecting currents across a cryostat wall, thus enabling the direct excitation of an HTS rotor coil circuit. We report on the performance of an experimental prototype device and discuss the integration of this device as a novel brushless exciter for an 8-pole, 10 kW, synchronous HTS generator.

2. Excitation of HTS coils using a rotating HTS flux pump

Rotating HTS flux pumps have been studied by various recent authors [32–37]. The basic principle of this type of flux pump is shown in figure 1(a). The rotating flux pump comprises a series of permanent magnets (PMs) mounted upon the circumference of a cylindrical rotor, which rotates so that the magnets pass over a coated-conductor HTS stator. Flux traverses the HTS stator wire and a time-averaged DC output voltage is observed. This voltage drives a DC current to flow

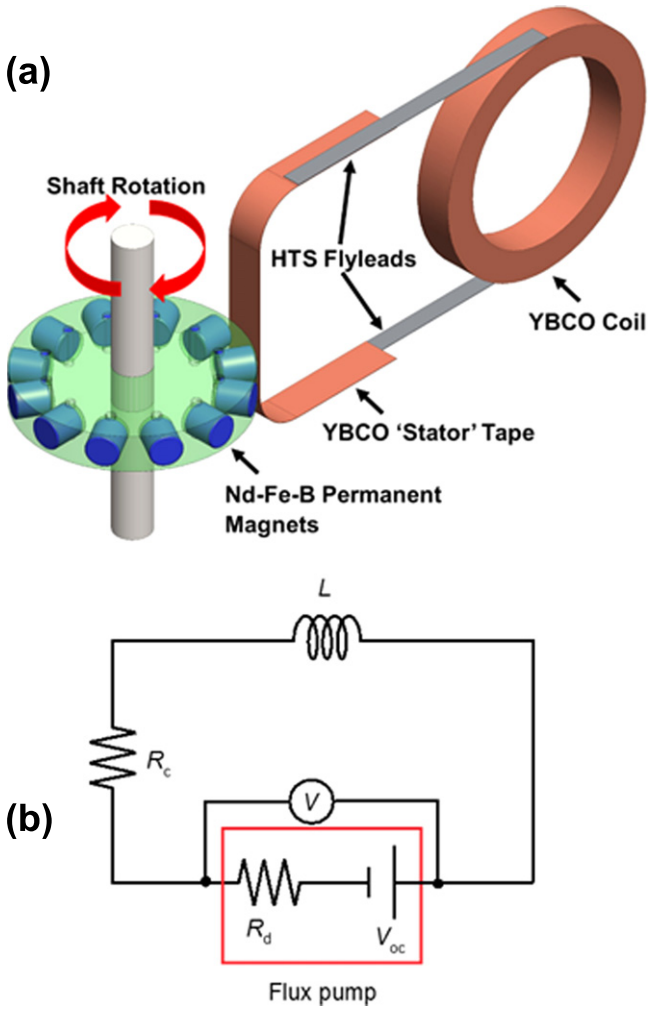

Figure 1. (a) Illustrative diagram showing basic design of previously reported rotating HTS flux pumps. (b) Equivalent circuit diagram of a superconducting circuit comprising an HTS coil of inductance L, connected in series with rotating HTS flux pump which outputs an open-circuit voltage, V_{oc}, and has an internal resistance R_d. R_c denotes the total circuit resistance due to normal soldered joints between the HTS wires.

around a series-connected circuit, and this current can become very large if the resistance of the series-connected circuit, R_c, is very low (see figure 2). We have recently demonstrated that the operation of these devices at a fixed frequency can be modelled [33, 34] as a simple DC voltage source with a constant open-circuit voltage, V_{oc}, and an effective internal resistance, R_d (see equivalent circuit shown in figure 1(b)). V_{oc} is observed to be proportional to the frequency of magnet crossings over the HTS stator wire, whilst R_d is attributed to the effect of *dynamic resistance* [38, 39] due to the oscillating magnetic field experienced by the HTS stator wire. The HTS circuit is completed using normal soldered joints which have a total resistance R_c, so that the total resistance of the circuit is given by the sum of $R_d + R_c$. It should be noted that whilst a robust experimental description of these devices is now available, the detailed microscopic physics which causes the generation of the DC voltage is still not well understood [34]. However if the engineering parameters V_{oc} and R_d are known for a specific flux pump, then the equivalent circuit in

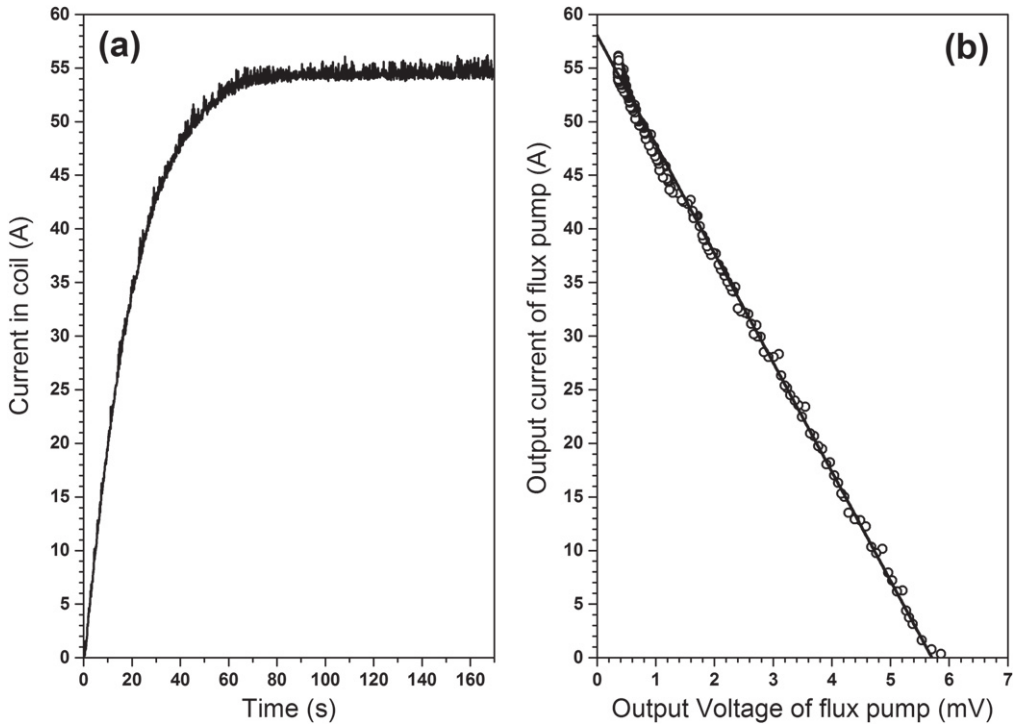

Figure 2. Typical performance plots for a rotating HTS flux pump of the type shown in figure 1(a) (based on data reported in [34]). (a) Time-evolution of current in a series-connected HTS coil ($L = 2.4$ mH, $R_c = 0.88$ $\mu\Omega$) during ramping excitation by a rotating HTS flux pump. The flux pump is turned 'on' at $t = 0$ s. (b) Measured output voltage versus output current from the rotating HTS flux pump for the coil-ramping run shown in figure 2(a).

figure 1(b) allows the performance of the flux pump to be predicted when connected to coil of arbitrary inductance, L.

The charging behaviour of a coil when connected in series with a DC voltage source (i.e. the rotating flux pump) is described by:

$$V_{oc} - I\left(R_d + R_c\right) = L\,\frac{dI}{dt}, \tag{1}$$

where t is the time elapsed following the start of operation of the flux pump. If $I = I_1$ at $t = 0$, then equation (1) implies:

$$I(t) = \left(I_1 - I_{max}\right)e^{-\frac{t}{\tau_\uparrow}} + I_{max}, \tag{2}$$

where $I_{max} = \frac{V_{oc}}{R_d + R_c}$ and $\tau_\uparrow = \frac{L}{R_d + R_c}$. Here, I_{max} represents the maximum current that can be injected into the circuit by the flux pump. The time, $t_\uparrow$, taken to increase the current in the circuit from I_1 to I_2 (where $I_2 > I_1$), is then given by:

$$t_\uparrow = \tau_\uparrow \ln\left[\frac{I_{max} - I_1}{I_{max} - I_2}\right]. \tag{3}$$

Hence, we see that the charging time is inversely proportional to the total resistance of the circuit. It is important to note that when the flux pump is turned off, both V_{oc} and R_d then equal zero. The time, $t_\downarrow$ for current in the circuit to decay back from I_2 to I_1 is then given by:

$$t_\downarrow = \tau_\downarrow \ln\left[\frac{I_2}{I_1}\right], \tag{4}$$

where $\tau_\downarrow = \frac{L}{R_c}$. If $R_c \ll L$ then the decay time can become very large. Reported values [40, 41] for lap solder joints between coated-conductor HTS wires range from <10 nΩ [42] up to >500 nΩ [43]. Our practical experience is that values <100 nΩ can be readily achieved with 4 mm Cu-coated YBCO wire.

A key limitation of the previously reported HTS rotating flux pumps, is that their design dictates that the flux pump rotor must be located within the cryogenic envelope. This is necessary because the output voltage is found to drop rapidly as the flux gap between the rotor magnet and HTS stator wire increases. In practice, the flux gap cannot be more than a few millimetres if these devices are to operate effectively [34]. However, placing the flux pump rotor within the cryostat has several major disadvantages. Firstly, it diminishes the thermal advantages of the flux pump, as this arrangement requires that the cryostat wall is now penetrated by a drive-shaft, which itself forms a heat conduction path into the cryostat. Secondly, rotating parts within the cryostat can lead to turbulence and friction heating. Thirdly, expensive and hard-to-maintain cryogenic bearings are required to mount the flux pump rotor in the cold environment. All of these issues could be eliminated if the flux pump rotor were mounted outside the cryostat so that the HTS circuit was excited through the cryostat wall. In this arrangement there are no penetrations of the cryostat wall, and all moving parts can be located at room temperature, thus significantly improving ease of maintenance. Importantly, the external-rotor arrangement is also well-suited to integration as a brushless HTS-PM exciter upon

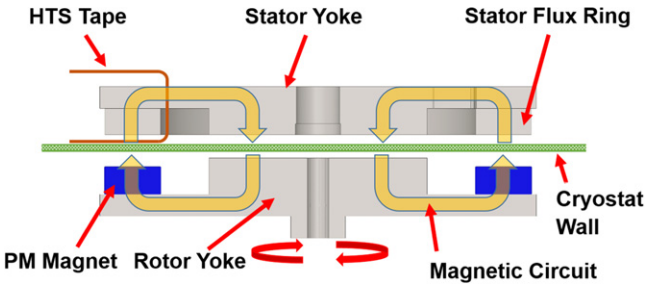

Figure 3. Schematic diagram showing the magnetic circuit formed between the ferromagnetic stator and rotor pieces within the experimental HTS-PM exciter.

an HTS generator or motor, as it can exploit the inherent rotation of the rotor cryostat.

In order to move the flux pump rotor outside the cryostat, the flux gap must be increased to a distance which is large enough to accommodate a thin cryostat wall (≳5 mm). This requires a new design approach which can realise an increased magnetic field at the HTS stator at these large flux gaps. One such approach is to employ ferromagnetic yoke pieces that form a magnetic circuit between the exciter-rotor and the exciter-stator. This arrangement enables flux to be focussed upon the coated-conductor stator wire. In the following sections, we report on the design and experimental characterisation of a novel HTS-PM exciter which adopts this approach.

3. Design and characterisation of a prototype externally-excited axial HTS flux pump

3.1. Experiment

Figure 3 shows a schematic of the magnetic circuit employed within our experimental HTS-PM exciter. Two shaped iron discs are used to form the main body of both the exciter-rotor and the exciter-stator. The rotor carries a series of 1″ × ½″ × ¼″ Nd–Fe–B permanent magnets (N42). When the iron pieces are placed on either side of a thin composite cryostat wall, a magnetic circuit is formed. Flux is focussed across the gap between the Nd–Fe–B magnets and the iron ring on the stator. The magnetic circuit is completed at the co-axial centre of the discs where flux is passed back across a gap between the rotor and stator. An HTS stator wire is introduced to the magnetic circuit by threading it through a hole in the iron stator yoke and wrapping the wire around the iron ring on the stator, so that perpendicular applied flux is focussed upon the coated-conductor wire. Figure 4 shows calculated values of the applied perpendicular magnetic field amplitude, B_{perp}, at the HTS stator wire as a function of flux gap, d. Also shown is B_{perp} due to an isolated Nd–Fe–B magnet of the same dimensions and magnetisation, which is similar to the applied fields used in the earlier reported rotating flux pump devices. It can be seen that for all flux gaps shown, the ferromagnetic circuit leads to a substantial increase in B_{perp} at the HTS stator wire. At a flux gap of

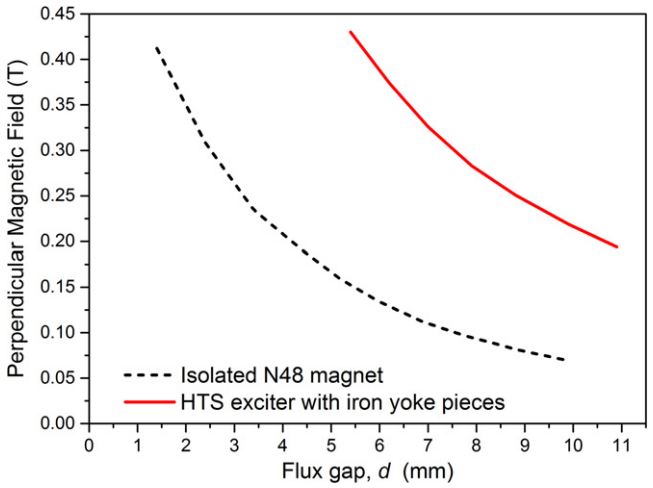

Figure 4. Plot of calculated applied perpendicular magnetic field, B_{perp} versus flux gap, d, at the HTS stator wire for the HTS exciter geometry shown in figure 2(a). The applied field obtained from an isolated N42 Nd–Fe–B magnet is also shown for comparison.

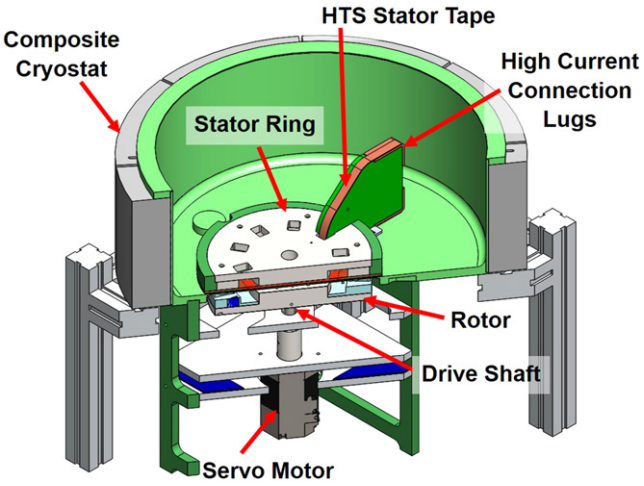

Figure 5. Schematic diagram of the externally-excited HTS rotating flux pump (HTS-PM exciter), incorporating iron yokes within rotor and stator pieces and flux return path.

5.4 mm, $B_{perp} = 0.43$ T at the exciter-stator. This exceeds the magnitude of B_{perp} obtained from the isolated PM magnet at a flux gap of 1 mm.

Figure 5 shows the apparatus used to experimentally characterise our prototype HTS-PM exciter. The iron stator yoke was placed on the base of a composite cryostat which was filled with liquid nitrogen. A length (180 mm) of YBCO coated-conductor stator wire was wrapped around the yoke ring. The YBCO wire was manufactured by Superpower Inc. and had a measured I_c of 255 A. The iron rotor carrying nine Nd–Fe–B magnets was mounted beneath a flat bottomed composite cryostat and a drive shaft connected the rotor to a speed-controlled servo-motor. The rotor was arranged to rotate parallel to the bottom surface of the cryostat with the Nd–Fe–B rotor magnets facing upwards. The flux gap between the external Nd–Fe–B magnets and the HTS stator

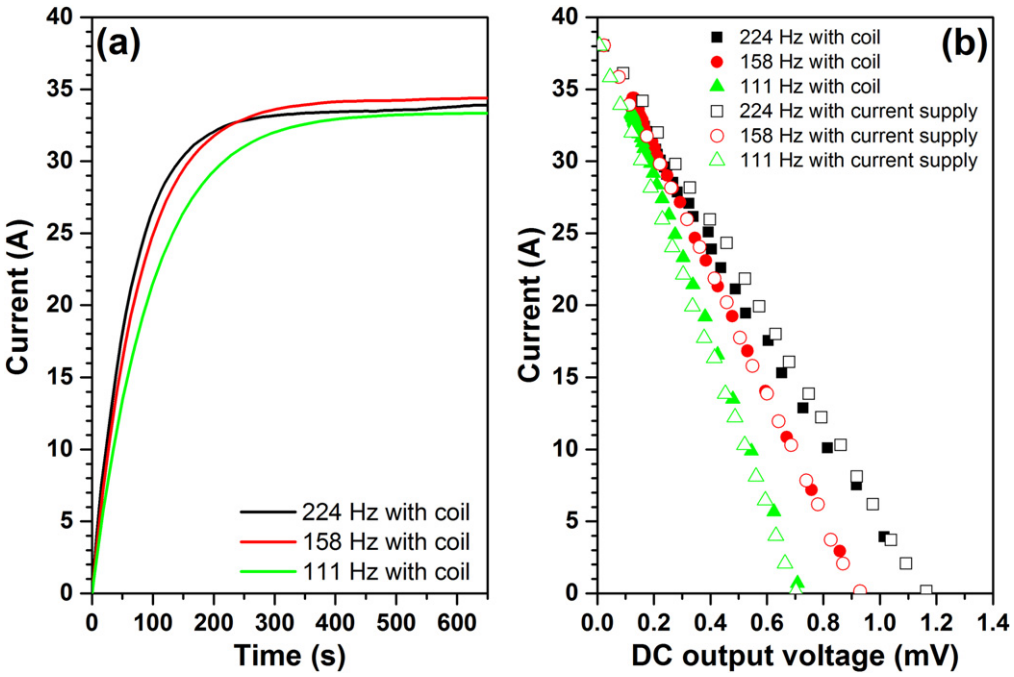

Figure 6. Experimental results from HTS-PM exciter using a flux gap of $d = 7.0$ mm. (a) Plot showing ramp-up of current measured in series connected HTS coil ($L = 1.97$ mH) after HTS-PM exciter was turned on at $t = 0$ s. (b) Plot showing equivalence of experimental *I–V* curves obtained using either a series connected HTS coil (Method 1—'with coil') or a calibrated current supply as a current-limiting load (Method 2—'with current supply').

wire inside the cryostat, could be varied through altering the height of the iron rotor using spacer plates of defined thickness. A thin (3 mm) sheet of G10 composite formed the section of the cryostat wall next to the rotor magnets. This enabled small flux gaps to be realised between the rotor magnets and the HTS stator wire. All measurements were made using a single coated-conductor stator wire which was soldered to large area copper connection lugs. Voltage taps were placed at either end of the stator wire and time-averaged voltage measurements were made over a sampling interval equal to ten rotation periods of the rotor.

Current–voltage performance curves were then acquired in one of two ways. In Method 1, a double pancake HTS coil was soldered in series with the HTS stator wire and the current in the circuit was monitored using a calibrated cryogenic Hall sensor (Arepoc HHP-NA) fixed at the centre of the coil. The HTS coil was wound from 4mm AMSC 2G wire and had an inductance, $L = 1.97$ mH and a critical current at the 1 μV criterion of $I_{c,coil} = 95$ A. In Method 2, a high stability current supply (Agilent 6680A-J04) was used to maintain a constant current in the HTS stator wire whilst the DC output voltage of the HTS-PM exciter was measured. Voltage measurements were made at current increments of 2 A. In this manner the calibrated supply acts as a fixed-current load for which the circuit current can be scanned across the full output range of the device. This method is identical to the approach widely used to obtain *I–V* performance curves from experimental photovoltaic devices [44]—which are also a type of DC voltage source with an internal impedance.

3.2. Results

The experimental HTS-PM exciter was operated at various different flux gaps and operating frequencies, and the DC output voltage was measured as a function of current through the HTS stator wire in each case. Figure 6(a) shows the evolution of current in a series-connected HTS coil (i.e. using Method 1) for three different operating frequencies of the HTS-PM exciter. (The operating frequency is the frequency at which rotor magnets cross the stator wire). In each case the current is observed to rise rapidly before stabilising at the asymptotic limit, I_{max}. This is consistent with equation (2). Figure 6(b) shows a comparison between data obtained using Method 1 (with coil) and Method 2 (with current supply). The 'with coil' data corresponds to the same experimental run as shown in figure 6(a). It can be seen that there is very close agreement between the data obtained using the two different experimental methods.

Having established the equivalence of the two characterisation methods we then proceeded to fully characterise the experimental HTS-PM device using Method 2, as this approach enabled data to be collected much more quickly and efficiently than Method 1. This was particularly the case at large flux gaps and low operating frequencies, where the time required to ramp the current in the HTS coil became impractically long.

Figure 7(a) shows the performance of the exciter at a flux gap of 5.4 mm for a range of different operating frequencies obtained using Method 2. The HTS-PM exciter exhibits a linear *I–V* relationship described by $V = V_{oc} - IR_d$ at all frequencies measured. This behaviour is consistent with

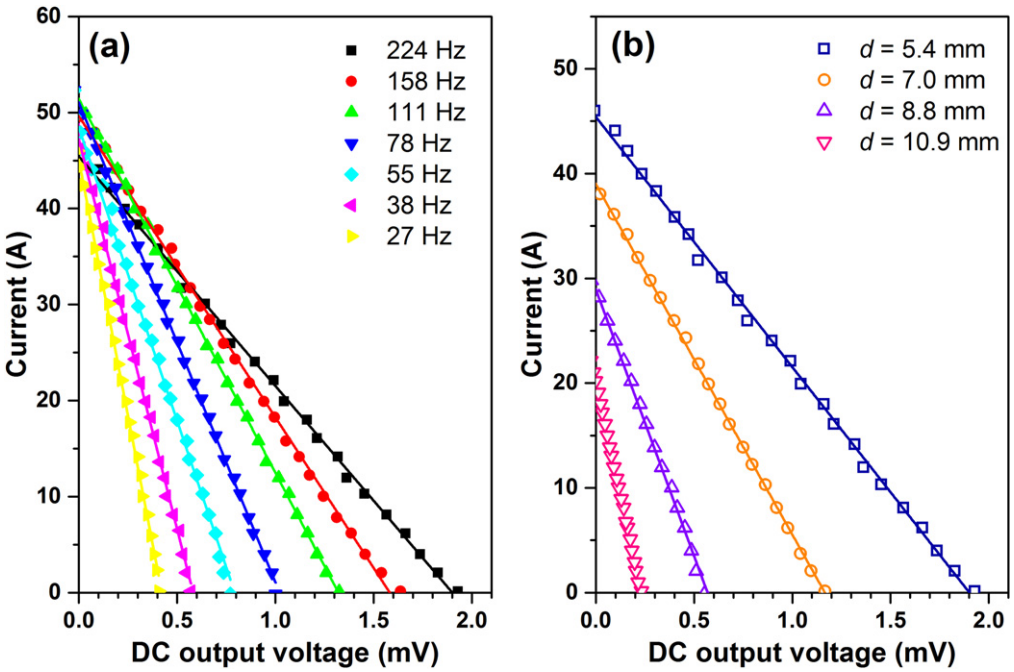

Figure 7. Experimentally-measured current–voltage plots for the prototype HTS-PM exciter reported here. (a) *I–V* plots at a flux gap of 5.4 mm for various operating frequencies. (b) *I–V* plots at $f = 224$ Hz for various flux gaps.

previously reported rotating flux pumps [33, 34]. Linear fits to the data are shown for each frequency. V_{oc} is obtained from the x-axis intercept, whilst the gradient of the line is equal to $-1/R_d$. The y-axis intercept gives the short-circuit current, $I_{sc} = V_{oc}/R_d$. It is important to note that I_{sc} represents the maximum current that can be injected into a superconducting coil from a single stator wire of the HTS-PM exciter. (I_{sc} is the output current at which the DC voltage dropped across the internal resistance of the stator wire is equal to the DC voltage generated across the wire). Figure 7(b) shows current–voltage plots for four different flux gaps at an operating frequency of 224 Hz. We observe that V_{oc}, I_{sc} and R_d all drop markedly as the flux gap is increased above 5.4 mm, however the device continues to operate at flux gaps of up to at least 10.9 mm.

Figure 8 shows plots of the values of V_{oc}, I_{sc} and R_d extracted from data obtained at each flux gap, d, and operating frequency, f. The open circuit voltage, V_{oc} rises with increasing frequency, but is not directly proportional to frequency. This is a point of difference with the previously reported flux pumps, where both V_{oc} and R_d were linearly correlated with frequency [33, 34]. We attribute this difference to the presence of eddy currents within the solid iron yoke employed in the exciter-stator used here. The effective internal resistance, R_d, also rises with frequency. The short-circuit current, $I_{sc} = V_{oc}/R_d$ is found to be a slowly rising function of frequency at large flux gaps. However at the smallest measured flux gap of 5.4 mm, I_{sc} is observed to peak at ~111 Hz before dropping at higher frequencies. Again, we attribute this to the presence of eddy currents which cause V_{oc} to decrease by a larger extent than R_d in this smaller flux gap. In principle eddy currents could be eliminated through the use of laminated or composite yokes, although this has not been studied here. If eddy current effects were eliminated, we would expect V_{oc} to be a linear function of frequency, and I_{sc} to rise to an asymptotic limiting value at high frequency for each flux gap [33, 34].

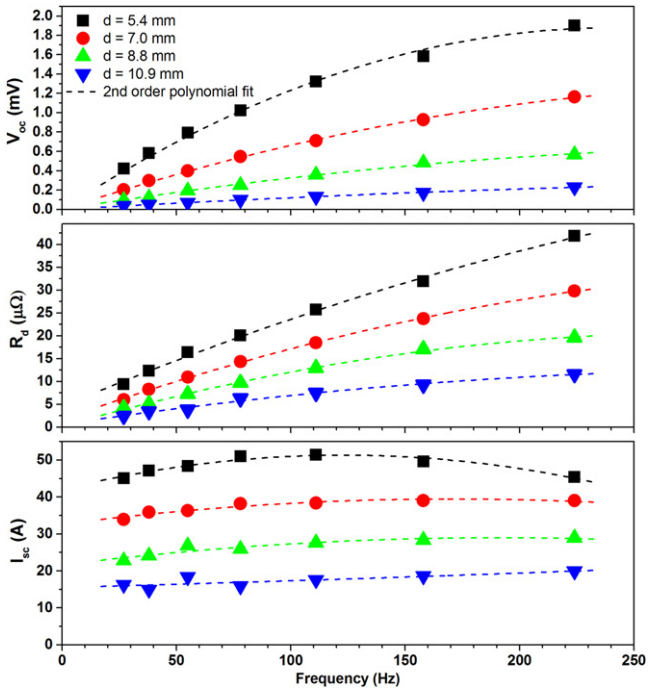

Figure 8. Plots showing experimentally-measured values of V_{oc}, R_d and I_{sc} for the experimental HTS-PM exciter obtained over a range of operating frequencies and flux gaps. Dotted lines show 2nd order polynomial fits which describe the frequency-dependence of the data over the range of values measured.

These experimental results clearly show that the HTS-PM exciter can operate across a cryostat wall, and that the

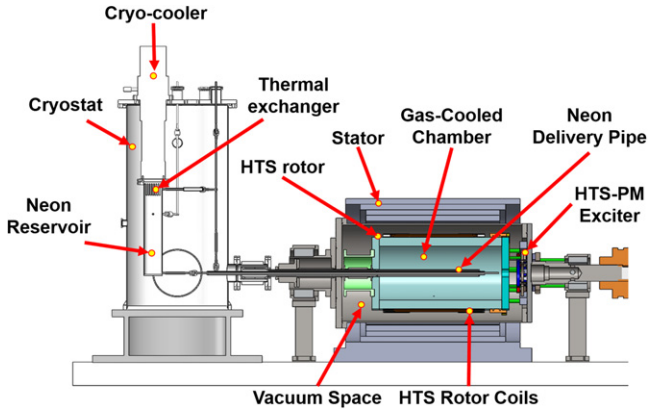

Figure 9. Diagram of the demonstration 10 kW HTS generator with integrated HTS-PM exciter.

exciter can output currents of >50 A per stator wire. Importantly, the measured experimental values for V_{oc}, R_d and I_{sc} now allow the performance of this experimental device to be calculated (from equations (1) to (4)) when connected in series with an HTS coil of known inductance. In the next section we use this approach to develop the design of a prototype HTS-PM exciter which will be integrated with a demonstration HTS generator.

4. Implementation of a flux pump exciter upon a 10 kW HTS generator

Figure 9 shows a schematic diagram of the prototype 10 kW, 8-pole, 200 rpm synchronous HTS generator [45] which is currently under construction at Changwon National University. Table 1 gives key specifications for the rotor of this machine. The generator rotor comprises eight double pancake racetrack HTS rotor coils wound from 4 mm coated conductor wire [46] manufactured by Sunam Co. Ltd. Cryogenic cooling of the rotor coils to 30 K is achieved through closed-cycle pumping of liquid neon from an ancillary cryo-cooler system. The rotor coils are connected in series, with a rated current of 85 A and a total series-connected self-inductance of 0.576 H.

This generator will provide a demonstration test-bed for the integration of an HTS-PM exciter based upon the experimental device discussed in section 3. Figure 9 shows how the HTS-PM exciter integrates with the generator rotor. The exciter-stator is fixed inside the rotating cryostat of the generator and as a result, the exciter-stator actually rotates in the laboratory frame of reference. The exciter-rotor is arranged to rotate coaxially with the generator rotor, but independently from it. This enables the relative rotational velocity between the exciter-rotor and exciter-stator to be varied, thus controlling the operating frequency of the exciter. In this demonstration system, the iron yoke of the exciter-stator will be coupled to the main cooling system via weak thermal links which ensure that the exciter-stator maintains a rated operating temperature of ~75 K. In future designs, a more thermally-efficient arrangement may be implemented in which the 75 K exciter-stator is cooled by a separate circuit which

Table 1. Design parameters of the double pancake coils (DPCs) for each of the eight rotor poles.

Rotor Coil Parameters	Value
Coil Type	Racetrack Double Pancake
Conductor type	REBCO (HTS)
Operating current	85 A
Operating temperature	30 K
Current margin (% of coil I_c)	60%
Number of turns	243 turns
Width of HTS wire	4 mm
Thickness of wire	0.14 mm
Length of wire	381 m
Inductance	79 mH

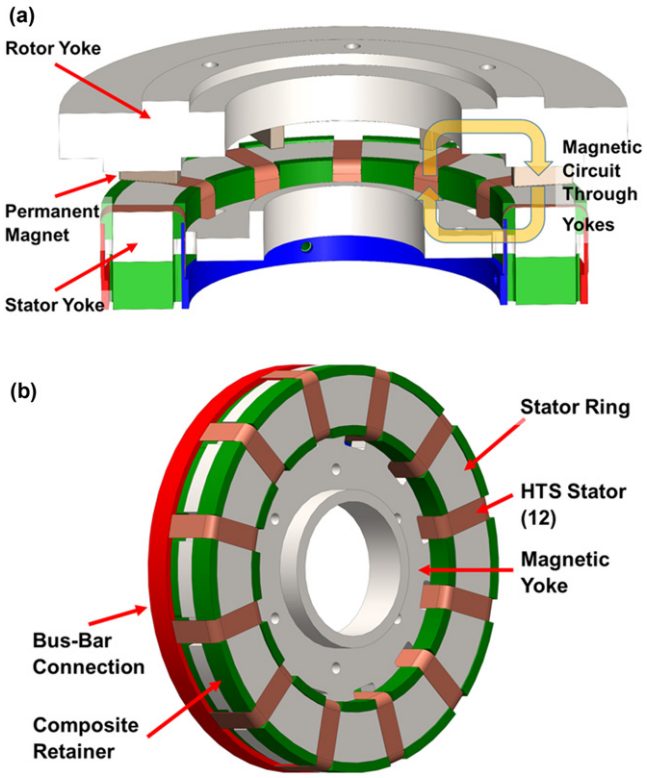

Figure 10. Detailed diagram of the integrated HTS-PM exciter showing iron yoke design and magnetic circuit between exciter-stator and exciter-rotor. (a) Cross-sectional view of the full HTS-PM assembly. The cryostat wall has been omitted for clarity. (b) View of the HTS-PM exciter stator only. Diagram shows 12 HTS stator wires passing around the iron yoke.

couples directly to the first stage of the cryo-cooler. Figure 10 shows a close-up view of the design of the integrated HTS-PM exciter, showing the magnetic circuit formed between the rotor and stator yoke pieces. The geometry of the integrated HTS-PM exciter and the rated operating temperature closely match the values employed in the experimental tests in section 3. This enables the expected performance of the integrated exciter to be modelled using our experimental test data.

The cryostat wall between the exciter-rotor and the exciter-stator is manufactured from a thermally insulating

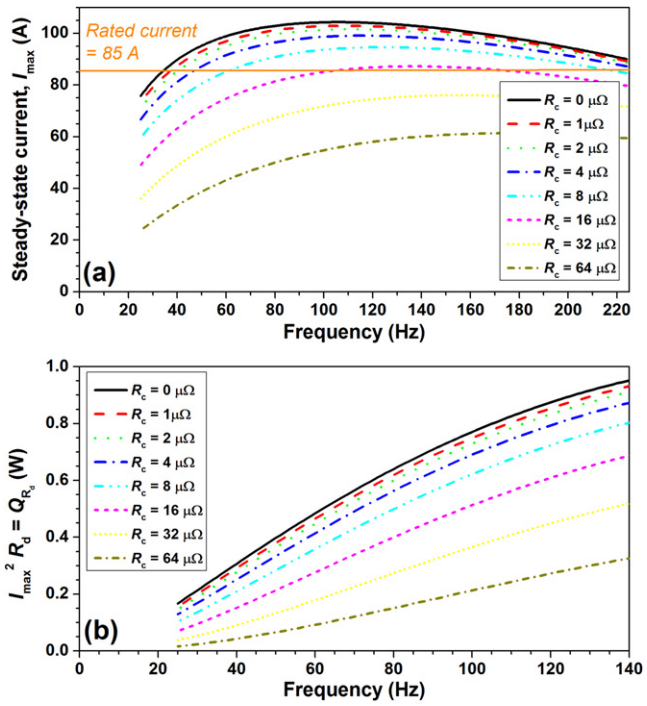

Figure 11. Calculated steady-state output of an HTS-PM exciter in 6S-2P configuration. (Calculations using 2nd order polynomial fits shown in figure 8): (a) steady-state output current, I_{max} as a function of operating frequency, f , and total circuit resistance, R_c. (b) Electrical heat load dissipated due to internal resistance of exciter stator, Q_{R_d}, plotted as a function of frequency for different values of total circuit resistance, R_c.

composite (G10) sandwich with a total width of 5 mm. Allowing for mechanical tolerances and clearance, this enables the HTS-PM exciter to operate at a minimum flux gap of $\geqslant$5.4 mm. The exciter-stator is designed to carry up to 12 coated conductor wires which can be connected in any series or parallel combination. This provides flexibility to match the output current and voltage of the HTS-PM exciter to the rotor circuit. A key requirement is that the maximum output current, I_{sc}, of the integrated exciter must exceed the rated current of the rotor coils (i.e. 85 A). The results from our experimental device (figure 8) indicate that this requires at least two parallel stator wires at $d = 5.4$ mm (or three equivalent parallel paths at $d = 7.0$ mm). By including additional series-connected stator wires in each equivalent parallel path, we can also increase the open-circuit voltage of the flux pump. This reduces the total time required to ramp the current in the rotor coils. As such, here we consider an arrangement of two parallel HTS paths upon the exciter-stator, each containing six wires in series. We adopt the naming convention 6S-2P to describe this configuration.

The steady-state output current of the exciter, I_{max}, is affected by the total series resistance of the rotor coil circuit, R_c. (R_c occurs due to the presence of normal-conducting soldered joints between the coils and the exciter). Figure 11(a) shows how I_{max} varies with R_c for a 6S-2P exciter integrated at a flux gap of 5.4 mm. I_{max} is the asymptotic limiting current when ramping current at a fixed operating frequency (see equation (2)). This means that the circuit can only attain a current of I_{max} if it is first energised to a higher current and then allowed to decay back to the equilibrium value. In practice this means that the rotor coils are likely to be energised using the largest value of I_{max} available (i.e. at a frequency of ~111 Hz) as this will reduce ramp-up times in all cases.

The rotor circuit of the demonstration generator contains nine soldered splices, and there are further soldered joints required to connect the stator wires within the flux pump exciter. Allowing for very conservative manufacturing tolerances, we can expect individual joint resistances of <150 nΩ to be achieved in all cases. This implies that the total series resistance of the closed rotor circuit, $R_c \leqslant 2\ \mu\Omega$. Using this value, figure 11(a) shows that a continuous operating frequency of >42 Hz will be required to maintain the rated rotor current of 85 A. Figure 11(a) also shows that for values of $R_c \leqslant 2\ \mu\Omega$, the total circuit resistance has little effect on the output of the HTS-PM exciter. This is because the internal resistance of the exciter (R_d) is the dominant component of the circuit resistance in this regime. In fact, the exciter is capable of exciting the rotor coil circuit even for values of $R_c > 16\ \mu\Omega$, which substantially exceeds practically expected values for the HTS circuit.

Figure 11(b) shows the electrical power, $Q_{R_d} = {I_{max}}^2 R_d$, which is dissipated at 75 K by the internal resistance of the exciter. We see that for operating frequencies up to approximately 120 Hz, this heat load increases approximately linearly with frequency. At $R_c = 2\ \mu\Omega$, the electrical heat load dissipated within the exciter can be approximately described by the simple equation, $Q_{R_d} = Nf$ where $N = 7.4 \times 10^{-3}$ W Hz^{-1}. We see that $Q_{R_d} < 700$ mW for all frequencies at which the HTS-PM exciter outputs the rated current of 85 A.

The total heat load imposed upon the cryostat during constant-frequency operation of the exciter also includes hysteretic magnetisation losses within the HTS stator wires, and losses in the iron yoke due to magnetic hysteresis and eddy currents. In principle, eddy current losses can be eliminated through the use of laminates or other iron-epoxy composites, but hysteretic losses in the HTS wire (Q_{HTS}) and the iron stator-yoke (Q_{Fe}) are a fundamental feature of this device. Hysteretic losses impose heat loads on the cryogenic system which are proportional to f. As Q_{R_d} is also approximately proportional to f across the operating region of interest, we can approximate the total heat load (neglecting eddy current losses) as:

$$Q_{Total} = Q_{R_d} + Q_{Fe} + Q_{HTS} \approx \beta f, \tag{5}$$

where the coefficient β is a constant. We can calculate the HTS magnetisation loss due to the 12 coated-conductor wires upon the stator using the equation of Brandt [47], for a peak-to-peak oscillation amplitude in B_{perp} of 0.43 T. We find that $Q_{HTS}/f = 189$ mW Hz^{-1}, such that $Q_{HTS} = 21$ W at 111 Hz. We can also estimate a highly conservative upper limit for the hysteretic iron loss in the stator by considering the transformer loss for an equivalent mass of laminated steel [48]. (This is a substantial over-estimate as much of the iron

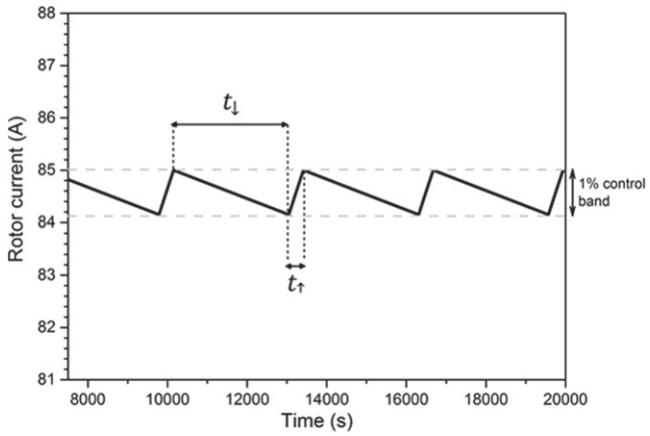

Figure 12. Plot illustrating current in rotor coil under duty-cycle control within a 1% control band from 85 A ($\alpha = 0.99$).

yoke comprising the exciter-stator does not experience the full oscillating field amplitude.) In this manner we obtain an upper limit of $Q_{Fe} < 0.2$ W at $d = 5.4$ mm and $f = 111$ Hz. This is negligible when compared to the HTS hysteresis loss. Substituting these values into equation (5) we obtain a value of $\beta \approx 0.2\,\mathrm{W\,Hz^{-1}}$. Under constant frequency operation at 42 Hz (for $R_c = 2\,\mu\Omega$) this indicates that $Q_{Total} = 7.9$ W.

However, it is important to recognise that power is not dissipated in the exciter-stator whilst the HTS-PM exciter is turned 'off' (i.e. the rotation speed is matched to the rotor, or the flux gap is greatly increased). When the exciter is 'off', current will decay in the circuit according to equation (4). From the total inductance of the rotor circuit, $L = 0.576$ H, and for $R_c = 2\,\mu\Omega$ we find that the decay time constant of the rotor coil circuit, $\tau_\downarrow > 80$ h. This long decay time enables the adoption of a 'duty-cycle' control loop which considerably reduces the total power dissipated within the cryostat. In this mode of operation, duty-cycle control maintains the rotor current within a control band between I_2 and I_1 ($I_2 > I_1$) by turning the exciter 'on' and 'off' as required. This is illustrated in figure 12 for the case when $I_1/I_2 = 0.99$ and $I_2 = 85$ A (i.e. a 1% control band). The duty cycle ratio, D, required to maintain the coil current within a given control band can be calculated from equations (3) and (4):

$$D = \frac{t_\uparrow}{t_\uparrow + t_\downarrow} = \frac{\tau_\uparrow \ln[\alpha]}{\tau_\uparrow \ln[\alpha] - \tau_\downarrow \ln\left[\dfrac{1-\alpha\gamma}{1-\gamma}\right]}, \qquad (6)$$

where $\alpha = I_1/I_2$ and $\gamma = I_2/I_{max}$. Figure 13(a) shows values obtained for $t_\uparrow$ and $t_\downarrow$ at $\alpha = 0.99$ (i.e. a 1% control band) as a function of the total series resistance. This data has been calculated for the 6S-2P configuration operating at 111 Hz. At $R_c = 2\,\mu\Omega$, we obtain $t_\downarrow = 2900$ s and $t_\uparrow = 360$ s. Figure 12 shows that the control loop follows a 'saw-tooth' profile in which the current changes approximately linearly with time during both ramping and decay. As a result, the duty cycle, D is independent of α, and is limited only by the switching time required to start and stop the exciter. In principle, duty cycle operation within a control band of less than 0.05% (i.e. $\alpha > 0.9995$) should be achievable for the conditions considered here.

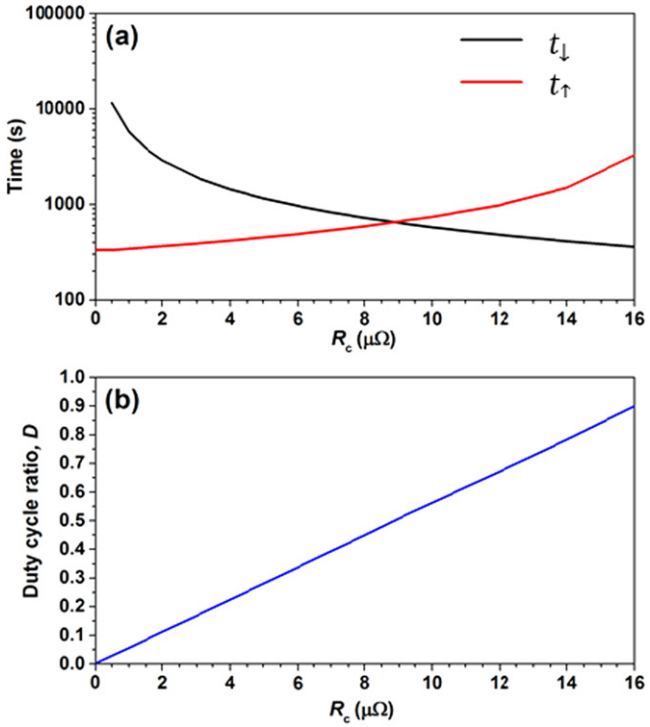

Figure 13. (a) Plot showing charge and discharge times of rotor circuit under duty cycle operation as a function of R_c. (Values calculated for an integrated 6S-2P flux exciter at $d = 5.4$ mm, $f = 111$ Hz, at $\alpha = 0.99$) (b) Calculated duty cycle ratios as a function of total series resistance, R_c.

Figure 13(b) shows that the duty cycle ratio, D, is proportional to R_c across the entire operating region, rising to $D = 1$ at the threshold value of $R_c = 18.7\,\mu\Omega$, at which the exciter can just output the rated current of 85 A during constant frequency operation. At $R_c = 2\,\mu\Omega$, a duty cycle ratio of $D = 0.112$ is required to maintain 85 A. The time-averaged heat load under duty cycle operation is then given by, $\overline{Q_{Total}} = D\beta f = 2.3$ W. This is substantially lower than the heat load calculated for constant frequency operation at the same R_c value (7.9 W). It is important to note that $\overline{Q_{Total}}$ is directly proportional to the duty cycle, and hence is also directly proportional to R_c. As a result, a more ambitious manufacturing specification of $R_c < 500\,\mathrm{n\Omega}$ would lead to a time averaged heat load of <0.6 W. (A value of $R_c < 500\,\mathrm{n\Omega}$ requires an average HTS lap joint resistance of less than $\sim 40\,\mathrm{n\Omega}$ which is achievable [42] at the coil temperature of 35 K.) For comparison, the optimised cryogenic heat load due to a pair of conventional 85 A copper current leads bridging between 300 K and 75 K is calculated [7] to be approximately 3.4 W.

A final issue to be discussed, is the time required for intial ramp-up excitation of the rotor coils during start-up of the generator. The very low output voltage of the HTS-PM exciter means that this initial ramp-up cannot happen quickly, and equation (3) determines the time required to ramp the rotor coils from 0 A to 85 A. Using the 6S-2P configuration at

111 Hz and an R_c of 2 nΩ, we find that the initial charge time is 221 min (=3.7 h). This is reasonable in the context a one-off start-up procedure. Once the rotor coils have been initially energised they will be kept cold and maintain rated operating current in the circuit at all times (unless an emergency shut-down occurs). In this aspect, duty-cycle operation of the HTS-PM exciter closely mimics the persistent-current operation of LTS magnets, such as those found in commercial MRI magnets.

5. Concluding remarks

In this work we have demonstrated the operation of a prototype HTS-PM exciter which enables the excitation of a closed HTS circuit. This exciter does not require metal current leads which penetrate the cryostat wall nor a bulky external power supply. This fundamentally alters the heat load imposed upon the cryogenic system. We have reported experimental results from a laboratory prototype, and shown that the device behaves as a constant voltage source with an effective internal resistance, and that typical output voltages are in the mV range per stator wire. This behaviour is similar to previously reported 'rotating HTS flux pump' devices. However we suggest that eddy currents which occur within the bulk iron yoke of our device, are the cause of diminished performance at high frequencies. Fortunately, the solution to this problem is well-known, and laminations or epoxy-iron composites should reduce this effect to a negligible level.

We have then shown how this device can enable the design of ultra-low loss generator rotors which do not require complex and maintenance-intensive high-current slip-rings to transfer current from an external power supply. We have discussed this in the context of the design integration of a brushless HTS-PM exciter within a 10 kW synchronous HTS generator. We have emphasised the value of appropriate design choices for the configuration of series and parallel connections of wires within the exciter-stator. Our modelling shows that the maximum output current of the exciter may be limited by the total circuit resistance, R_c, which occurs due to soldered joints between coated-conductor wires. This is a result of the rather low output voltage developed by the exciter. Nonetheless, in the case considered here, the use of a 6S-2P configuration allows comparatively large values of R_c ($>16\ \mu\Omega$) to be overcome. We have also emphasised the importance of minimising R_c in order to minimise the total heat load imposed by the HTS-PM exciter upon the cryogenic system. Importantly, adopting a duty cycle operating mode enables the HTS-PM exciter to be 'turned off' for long periods and this can lead to a large reduction in the total power dissipated within the exciter-stator. In order to operate at low duty-cycle ratios it is necessary to manufacture rotor coil circuits with low total series resistance. In the case considered, we find that a value of $R_c = 2\ \mu\Omega$ leads to a total heat load on the cryostat which is approximately ⅔ of that expected from conventional current leads. Furthermore, a value of $R_c < 500$ nΩ would enable rotor circuit operation at 85 A to be maintained whilst dissipating <0.6 W within the rotor cryostat. This is less than 20% of the heat load imposed by equivalently rated copper current leads.

Our modelling indicates that hysteretic HTS magnetisation loss within the coated-conductor stator wires comprises >80% of the total calculated heat load. Minimising the number of stator wires could enable the heat load to be further reduced, however there is a trade-off with achieving practical ramping times for a specified rotor coil circuit. Future work will include optimisation of the number and configuration of coated-conductor wires required for a given application.

The assembly, commissioning and demonstration of the 10 KW demonstration HTS generator described in this paper is currently underway at Changwon University and is scheduled be completed by the end of 2016.

Acknowledgments

This work was supported by the New Zealand MBIE Contract No. RTVU1402, and the Power Generation & Electricity Delivery Core Technology Program of the Korea Institute of Energy Technology Evaluation and Planning (KETEP), granted financial resource from the Ministry of Trade, Industry & Energy, Republic of Korea (No. 20142020103560).

References

[1] Abrahamsen A B, Mijatovic N, Seiler E, Zirngibl T, Træholt C, Nørgard P B, Pedersen N F, Andersen N H and Østergard J 2010 Superconducting wind turbine generators *Supercond. Sci. Technol.* **23** 034019

[2] Sivasubramaniam K, Zhang T, Lokhandwalla M, Laskaris E T, Bray J W, Gerstler B, Shah M R and Alexander J P 2009 Development of a high speed HTS generator for airborne applications *IEEE Trans. Appl. Supercond.* **19** 1656–61

[3] Miki M *et al* 2006 Development of a synchronous motor with Gd–Ba–Cu–O bulk superconductors as pole-field magnets for propulsion system *Supercond. Sci. Technol.* **19** S494–9

[4] Umemoto K *et al* 2010 Development of 1 MW-class HTS motor for podded ship propulsion system *J. Phys.: Conf. Ser.* **234** 032060

[5] Nick W, Frank M, Klaus G, Frauenhofer J and Neumüller H-W 2007 Operational experience with the world's first 3600 rpm 4 MVA generator at Siemens *IEEE Trans. Appl. Supercond.* **17** 2030–3

[6] Neumuller H W, Nick W, Wacker B, Frank M, Nerowski G, Frauenhofer J, Rzadki W and Hartig R 2006 Advances in and prospects for development of high-temperature superconductor rotating machines at Siemens *Supercond. Sci. Technol.* **19** S114–7

[7] Kalsi S S 2011 *Applications of High Temperature Superconductors to Electric Power Equipment* (Piscataway, NJ: IEEE Press)

[8] Barnes P N, Sumption M D and Rhoads G L 2005 Review of high power density superconducting generators: present state and prospects for incorporating YBCO windings *Cryogenics* **45** 670–86

[9] Kwon Y K, Kima H M, Baik S K, Lee E Y, Lee J D, Kim Y C, Lee S H, Hong J P, Jo Y S and Ryu K S 2008 Performance test of a 1 MW class HTS synchronous motor for industrial application *Physica* C **468** 2081–6

[10] Guina A, Kells J, Labes K, Sercombe D, Lissington T, Fuger R, Matsekh A and Geronimo C P F 2014 Electromagnetic turbine *International Patent Application* WO2014/040145
[11] Tsukamoto O 2014 Present status and future trends of R&D for HTS rotational machines in Japan *Physica* C **504** 106–10
[12] Ueno E, Kato T and Hayashi K 2014 Race-track coils for a 3 MW HTS ship motor *Physica* C **504** 111–4
[13] Oswald B, Best K-J, Soell M, Duffner E, Gawalek W, Kovalev L K, Krabbes G and Prusseit W 2007 HTS motor program at OSWALD, present status *IEEE Trans. Appl. Supercond.* **17** 1583–6
[14] Kim A-R *et al* 2015 Performance analysis of a 10 kW superconducting synchronous generator *IEEE Trans. Appl. Supercond.* **25** 5202004
[15] Karmaker H, Ho M and Kulkarni D 2015 Comparison between different design topologies for multi-megawatt direct drive wind generators using improved second generation high temperature superconductors *IEEE Trans. Appl. Supercond.* **25** 5201605
[16] Kummeth P, Nick W, van Hasselt P, Frank M, Kuhnert A, Oomen M and Arndt T 2015 Design and development of a test rig for HTS generator components *IEEE Trans. Appl. Supercond.* **25** 9500204
[17] Kalsi S S, Weeber K, Takesue H, Lewis C, Neumueller H-W and Blaugher R D 2004 Development status of rotating machines employing superconducting field windings *Proc. IEEE* **92** 1688–704
[18] Sung H-J, Park M and Yu I-K 2015 Designs of 10 MW air-core and iron-core HTS wind power generators *J. Electr. Eng. Technol.* **10** 545–50
[19] Ballarino A 2013 Current leads, links and buses *Proc. of the CAS-CERN Accelerator School: Superconductivity for Accelerators (Erice, Italy)* (doi:10.5170/CERN-2014-005.547)
[20] Alley D M, Hagen L J, Kuhlmann-Wilsdorf D, Makel D D and Moore C G III 1991 Automated apparatus for long-term testing of electrical brushes *IEEE Trans. Compon. Hybrids Manuf. Technol.* **14** 31–6
[21] Snitchler G, Gamble B and Kalsi S S 2005 The performance of a 5 MW high temperature superconductor ship propulsion motor *IEEE Trans. Appl. Supercond.* **15** 2206–9
[22] Ruuskanen V *et al* 2009 Modelling the brushless excitation system for a synchronous machine *IET Electr. Power Appl.* **3** 231–9
[23] Lawson D K and Dow T A 1985 The sparking and wear of high-current density electrical brushes *Wear* **102** 105–25
[24] Dow T A and Kannel J W 1982 Thermomechanical effects in high current density electrical slip rings *Wear* **79** 93–105
[25] Little D J 1991 Turbines, generators and associated plant *Modern Power Station Practise, Incorporating Modern Power System practise* vol C (Oxford: Pergamon)
[26] van Beelen H, Arnold A J P T, Sypkens H A, van Braam Houckgeest J P, De Bruyn Ouboter R, Beenakker J J M and Taconis K W 1965 Flux pumps and superconducting solenoids *Physica* **31** 413–43
[27] van de Klundert L J M and ten Kate H H J 1981 Fully superconducting rectifiers and fluxpumps I. Realized methods for pumping flux *Cryogenics* **21** 195–206
[28] Ferendeci A M, Mawardi O K, Melfi M J and Laquer H 1981 Flux pump excited brushless alternator *IEEE Trans. Magn.* **17** 146–8
[29] Bai Z, Yan G, Wu C, Ding S and Chen C 2010 A novel high temperature superconducting magnetic flux pump for MRI magnets *Cryogenics* **50** 688–92
[30] Fu L, Matsuda K, Baghdadi M and Coombs T 2015 Linear flux pump device applied to high temperature superconducting (HTS) magnets *IEEE Trans. Appl. Supercond.* **25** 4603804
[31] Ishmael S, Goodzeit C, Masson P, Meinke R and Sullivan R 2008 Flux pump excited double-helix rotor for use in synchronous machines *IEEE Trans. Appl. Supercond.* **18** 693–6
[32] Hoffmann C, Pooke D and Caplin A D 2011 Flux pump for HTS Magnets *IEEE Trans. Appl. Supercond.* **21** 1628
[33] Jiang Z, Hamilton K, Amemiya N, Badcock R A and Bumby C W 2014 Dynamic resistance of a high-T_c superconducting flux pump *Appl. Phys. Lett.* **105** 112601
[34] Jiang Z, Bumby C W, Badcock R A, Sung H-J, Long N J and Amemiya N 2015 Impact of flux gap upon dynamic resistance of a rotating HTS flux pump *Supercond. Sci. Technol.* **28** 115008
[35] Hoffmann C, Walsh R, Karrer-Mueller E and Pooke D 2012 Design parameters for an HTS flux pump *Phys. Proc.* **36** 1324–9
[36] Walsh R M, Slade R, Pooke D and Hoffmann C 2014 Characterization of current stability in an HTS NMR system energized by an HTS flux pump *IEEE Trans. Appl. Supercond.* **24** 4600805
[37] Coombs T A, Fagnard J F and Matsuda K 2014 Magnetization of 2 G coils and artificial bulks *IEEE Trans. Appl. Supercond.* **24** 8201005
[38] Oomen M P, Rieger J, Leghissa M, ten Haken B and ten Kate H H J 1999 *Supercond. Sci. Technol.* **12** 382–7
[39] Ogasawara K, Yasukochi K, Nose S and Sekizawa H 1976 *Cryogenics* **16** 33–8
[40] Park D K, Ahn M C, Kim H M, Lee H G, Chang K S, Lee S J, Yang S E and Ko T K 2007 Analysis of a joint method between superconducting YBCO coated conductors *IEEE Trans. Appl. Supercond.* **17** 3266–9
[41] Ito S and Hashizume H 2012 Transverse stress effects on critical current and joint resistance in mechanical lap joint of a stacked HTS conductor *IEEE Trans. Appl. Supercond.* **22** 6400104
[42] Sugano M, Nakamura T, Shikimachi K, Hirano N and Nagaya S 2007 Stress tolerance and fracture mechanism of solder joint of YBCO coated conductors *IEEE Trans. Appl. Supercond.* **17** 3067–70
[43] Sohn M H, Kim S W, Baik S K, Jo Y S, Seo M G, Lee E Y and Kwon Y K 2003 Joint resistances between two parallel high Tc superconducting tapes *IEEE Trans. Appl. Supercond.* **13** 1764–7
[44] ASTM E948-15 2015 *Standard Test Method for Electrical Performance of Photovoltaic Cells Using Reference Cells Under Simulated sunlight* (West Conshohocken, PA: ASTM International) (doi:10.1520/E0948-15)
[45] Sung H-J, Go B-S, Park M and Yu I-K 2015 Parameter tuning of a large-scale superconducting wind power generator for applying a flux pump *KIEE Summer Conf.* vol 7 15–7
[46] Lee J-H, Lee H, Lee J-W, Choi S-M, Yoo S-I and Moon S-H 2014 RCE-DR, a novel process for coated conductor fabrication with high performance *Supercond. Sci. Technol.* **27** 044018
[47] Brandt E H and Indenbom M 1993 *Phys. Rev.* B **48** 12893–906
[48] Sprague S 2015 *Magnetics Material Comparison* (California, USA: Proto Laminations Inc.)